Proton radius from electron-proton scattering and chiral perturbation theory

Marko Horbatsch,[1] Eric A. Hessels,[1] and Antonio Pineda[2]
[1]*Department of Physics and Astronomy, York University, Toronto, Ontario, Canada M3J 1P3*
[2]*Department of Physics and IFAE-BIST, Universitat Autònoma de Barcelona, E-08193 Bellaterra, Barcelona, Spain*
(Received 1 November 2016; published 13 March 2017)

We determine the root-mean-square proton charge radius, R_p, from a fit to low-Q^2 electron-proton elastic-scattering cross-section data with the higher moments fixed (within uncertainties) to the values predicted by chiral perturbation theory. We obtain $R_p = 0.855(11)$ fm. This number falls between the value obtained from muonic hydrogen analyses and the CODATA value (based upon atomic hydrogen spectroscopy and electron-proton scattering determinations).

DOI: 10.1103/PhysRevC.95.035203

The measurement [1,2] of the Lamb shift in muonic hydrogen, $E(2P_{3/2}) - E(2S_{1/2})$, and its associated determination of the root-mean-square electric charge radius of the proton,

$$R_p = 0.8409(4)\ \text{fm}, \tag{1}$$

has led to a lot of controversy. The reason is that this determination is 7.1 standard deviations away from the CODATA 2010 [3] value of $R_p = 0.8775(51)$ fm (and 5.6 standard deviations away from the updated CODATA 2014 [4] value of 0.8751(61) fm). The CODATA value is based on an average of determinations coming from hydrogen spectroscopy and from electron-proton scattering data.

Such a large discrepancy calls for an explanation. For the R_p value obtained from the Lamb shift in muonic hydrogen, the major criticism concerned the determination and error analysis of the two-photon-exchange contribution needed for obtaining R_p. On the one hand, dispersion relation analyses were used (see, for instance, Refs. [5–9]). These assume Regge behavior at large energies, which, at present, cannot be directly derived from QCD. They also require very precise knowledge of the elastic and inelastic form factors that enter into those dispersion relations, as in some cases very precise cancellations may occur. Nevertheless, the major concern is that momentum-dependent subtraction functions were needed to make the dispersion relation integrals convergent. Such functions cannot be deduced from experiment and therefore introduce some model dependence, which is difficult to quantify, as emphasized in Ref. [10].

Chiral perturbation theory avoids all of these issues in the calculation of the two-photon exchange contribution. This contribution is chirally divergent (linearly in $1/m_\pi$), and this linear divergence allows for a model-independent prediction for the two-photon-exchange term, which avoids the abovementioned dispersion relation analysis shortcomings. The two-photon-exchange contribution has been obtained in a series of papers [11–15]. The complete result can be found in Ref. [14], where not only the strict chiral result but also the leading contribution associated with the Δ particle (motivated in the large-N_c approximation of QCD) is incorporated.

The introduction of this result into the muonic hydrogen bound-state energy computation (which was done using effective field theory techniques, see Refs. [16–20]) produced the following value [21]:

$$R_p = 0.8413(15)\ \text{fm}. \tag{2}$$

This value has a larger uncertainty than Eq. (1), but, nevertheless, it eliminates the model dependence, giving a model-independent significance to the substantial discrepancy with the CODATA value.

The other side of the discrepancy comes from the CODATA average [3,4]. As mentioned, the CODATA value is an average of determinations coming from hydrogen spectroscopy and from electron-proton scattering. In this article we focus on the determination of R_p from the precise electron-proton scattering measurements of the MAMI Collaboration [22]. Their full analysis [23] leads to $R_p = 0.879(8)$, in variance with the muonic hydrogen value by 4.6 standard deviations.

The determination of R_p from electron-proton scattering data has been discussed extensively in the literature [23–40]. The proton radius can be determined [24] from scattering data from

$$R_p = \sqrt{-3\frac{d\sigma_{\text{red}}}{dQ^2}\Big|_{Q^2=0} + \frac{3\mu_p^2}{4m_p^2}}, \tag{3}$$

with

$$\sigma_{\text{red}} = (1+\tau)\frac{d\sigma}{d\Omega}\Big/\frac{d\sigma_{\text{Mott}}}{d\Omega} = G_{\text{E}}^2 + \frac{\tau G_{\text{M}}^2}{\epsilon}, \tag{4}$$

where $d\sigma_{\text{Mott}}/d\Omega$ is the Mott differential cross section,

$$\epsilon = \left[1 + \frac{4Q^2 + \frac{Q^4}{m_p^2}}{8E^2 - 2\frac{Q^2}{m_p}(2E + m_p)}\right]^{-1},$$

$\tau = Q^2/(4m_p^2)$, E is the electron energy, and $Q^2 = -(p_i - p_f)^2$, with p_i and p_f being the initial and final electron four-momenta. Here, m_p is the proton mass, $\mu_p = 2.792\,847\,4$ is the magnetic moment of the proton in units of nuclear magnetons, and we use units with $\hbar = c = 1$. Note that Eq. (3) follows from Eq. (4) because $\epsilon = 1$ at $Q^2 = 0$ for any energy E.

In principle, R_p could be determined from Eq. (3) from sufficiently precise measurements of $d\sigma/d\Omega$ at small Q^2, because only the leading terms of the Taylor expansions of the form factors,

$$G_{\text{E}}(Q^2) = 1 - \frac{R_{\text{p}}^2}{3!}Q^2 + \frac{\langle r^4\rangle_{\text{E}}}{5!}Q^4 - \frac{\langle r^6\rangle_{\text{E}}}{7!}Q^6 + \cdots \tag{5}$$

and

$$\frac{G_{\rm M}(Q^2)}{\mu_{\rm p}} = 1 - \frac{\langle r^2\rangle_{\rm M}}{3!}Q^2 + \frac{\langle r^4\rangle_{\rm M}}{5!}Q^4 - \frac{\langle r^6\rangle_{\rm M}}{7!}Q^6 + \cdots , \tag{6}$$

become necessary. However, with existing data, a functional form for the Sachs form factors $G_E(Q^2)$ and $G_M(Q^2)$ must be assumed to obtain a sufficiently accurate extrapolation of the measured data to $Q^2 = 0$. The first derivative of $G_M(Q^2)$ and the second derivative of $G_E(Q^2)$ at $Q^2 = 0$ (which are proportional to the magnetic and electric moments $\langle r^2\rangle_M$ and $\langle r^4\rangle_E$, respectively) are of particular importance in this extrapolation to $Q^2 = 0$.

One can find strong arguments for why one should focus on the low-Q^2 part of the data to extract the proton charge radius. The charged-pion-production threshold at $Q^2 = -4m_\pi^2 \approx -0.078$ GeV^2 results in a branch cut in the analytically continued form factor. Thus, one can seriously doubt attempts at fitting (by polynomials or other functions, such as splines) data beyond the value of $Q^2 = 0.078$ GeV^2 and having confidence in an accurate determination of the slope of $G_E(Q^2)$ at $Q^2 = 0$. Fits that include higher-Q^2 MAMI data [22] also require floating 31 normalization constants, and the floating of these constants leads to considerable flexibility in the fits, which also makes determination of the higher-order moments more difficult.

However, concentrating only on low-Q^2 data ($Q^2 < 0.078$ GeV^2) has not allowed for an accurate determination of R_p, because this data cannot determine the necessary higher moments (in particular, $\langle r^2\rangle_M$ and $\langle r^4\rangle_E$) to sufficient accuracy to allow for a precise extrapolation to $Q^2 = 0$ of the required first derivative of $G_E(Q^2)$ [Eq. (3)]. Thus, out of necessity, many attempts have been made to fit scattering data up to higher Q^2 to determine R_p while simultaneously determining the higher-order moments.

In Ref. [24], it was shown that values of R_p ranging from 0.84 to 0.89 fm are possible from acceptable fits of the MAMI data, with the value of R_p depending on the functional forms of G_E and G_M that are used for the extrapolation to $Q^2 = 0$. In particular, the higher moments assumed by the different functional forms lead to the wide range of R_p values. The implication of that work [24] is that a precise value of R_p cannot be obtained from electron-proton elastic scattering unless precise lower-Q^2 data become available or unless there are external constraints on the functional form of $G_E(Q^2)$ and $G_M(Q^2)$. The latter (external constraints on the functional forms—as obtained from chiral perturbation theory) is the main topic of this work.

As discussed above, the introduction of computations that incorporate the correct chiral structure and the associated power counting of the theory has allowed for a solution to the theoretical problems that the muonic hydrogen determination of R_p was facing, allowing for a model-independent determination of the two-photon exchange using pure chiral perturbation theory.

Here we investigate if a similar analysis can shed some light on electron-proton scattering, and, indeed, something similar happens here. Chiral perturbation theory determines the dominant (nonanalytic) dependence on the pion mass of the different moments. For $R_p^2 = \langle r^2\rangle_E$, one obtains only the logarithmic dependence, and therefore no accurate estimate can be made. For the higher moments, and all magnetic moments, however, one obtains answers for the moments that are in inverse powers of the pion mass, which allows for a determination of the leading term and an estimate of the uncertainty based on the estimated effect of missing higher terms. To obtain these moments, one needs the chiral expressions of the Sachs form factors, first obtained in Refs. [41–43]. The latter two references work in the heavy-baryon formalism to third order, which is the formalism that we use. Reference [43] also incorporates the Δ-particle effects into the computation. Below the threshold imposed by the branch cut ($Q^2 < 0.078$ GeV^2), these form factors are analytic and can be Taylor expanded. From the Taylor expansion and Eqs. (5) and (6), the moments can be determined. In Ref. [14], one can find analytic expressions for $\langle r^{2k}\rangle_E$ ($k > 1$). The expressions for $\langle r^{2k}\rangle_M$ are given in the Appendix of the present paper, where we also give the purely chiral result for the Sachs form factors in a compact form.

TABLE I. Values of $\langle r^n\rangle_E$ and $\langle r^n\rangle_M$ in units of fm from chiral perturbation theory. The first row is the pure chiral prediction (with only pions), and the second row is the result after the inclusion of the effects associated with the Δ particle. Uncertainties in the last two digits are shown in parentheses.

	$\langle r^4\rangle_E$	$\langle r^6\rangle_E$	$\langle r^8\rangle_E$	$\langle r^2\rangle_M$	$\langle r^4\rangle_M$	$\langle r^6\rangle_M$
π	0.71(36)	5.4(2.7)	104(52)	0.35(18)	0.71(35)	6.3(3.2)
π and Δ	0.60(29)	5.0(2.0)	99(37)	0.44(16)	0.79(28)	6.9(2.4)

Values (and uncertainties) obtained in this way for the lowest calculable electric and magnetic moments can be found in Table I. Note that in all cases the correction due to the Δ particle is quite small. The uncertainties in the first row of the table are estimated to be of order $m_\pi/\Delta \sim 1/2$, where $\Delta = m_\Delta - m_p$. The uncertainty in the chiral perturbation theory contribution in the second row is of order $m_\pi/(m_{\rm Roper} - m_p) \sim 1/3$, due to the Roper resonance. This estimate is also large enough to include corrections of order m_π/m_ρ, where m_ρ is the mass of the ρ meson. Finally, the uncertainty of the contribution due to the Δ included in the second row is estimated to be of order $1/N_c$ (where $N_c = 3$ is the number of colors). In practice, we take the more conservative estimate of $1/2 \sim \Delta/(m_{\rm Roper} - m_p)$. A detailed discussion of the uncertainty analysis is given in Ref. [14]. The overall uncertainty in the moments given in the final row of Table I is approximately 30 to 40%.

To determine R_p, we fit the lowest-Q^2 MAMI data using Eqs. (5) and (6) [along with Eq. (4)], but fix the moments, $\langle r^{2k}\rangle_E$ (for $k \geqslant 2$) and $\langle r^{2k}\rangle_M$ (for $k \geqslant 1$), to be their predicted values (second row of Table I) from chiral perturbation theory (to within their uncertainties), while performing a least-squares fit to determine R_p. The value of $\langle r^2\rangle_E \equiv R_p^2$ is the only moment which chiral perturbation theory cannot determine with sufficient accuracy, and thus it must be determined from fitting to the data.

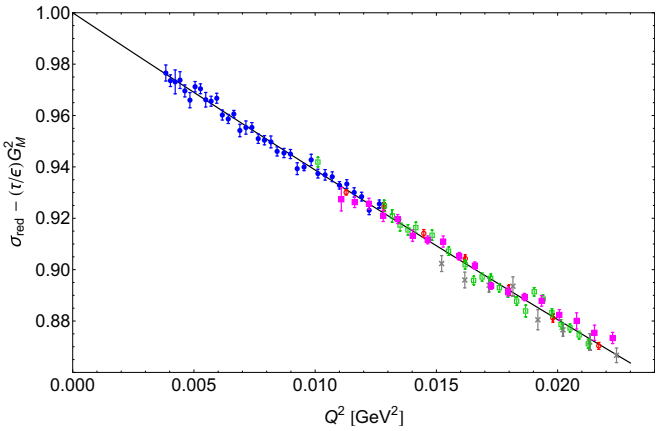

FIG. 1. Shown is the fit of the MAMI data [22] up to $Q^2_{max} = 0.023$ GeV^2 (the largest Q^2_{max} value considered in this work). The quantity plotted is the experimental cross section, scaled as in Eq. (4), with the contribution from the magnetic form factor (as predicted from chiral perturbation theory) subtracted out. The derivative of this quantity with respect to Q^2 at $Q^2 = 0$ gives the value of R_p [Eq. (3)]. The fit uses the functional forms of Eqs. (5) and (6), with R_p floating and the higher moments set to the values of Table I. The different symbols (colors) represent separate data groups, with the closed circles (blue), open circles (red), and open squares (green) data taken at an energy of 180 MeV, the closed squares (magenta) at 315 MeV, and the crosses (gray) at 450 MeV. Each group has a separate normalization constant that must also float in the fit. Repeated measurements within a data group at identical (or nearly identical) Q^2 values have been averaged only for the purpose of aiding the clarity of the presentation.

Our fitting procedure follows that described in Ref. [24]. Before performing the fits, we remove the Feshbach two-photon-exchange correction and replace it with the more complete two-photon-exchange correction calculated following the prescription of Ref. [44]. For the low-Q^2 data used in this work, these corrections agree well with the low-Q^2 two-photon-exchange calculations of Ref. [45]. In fact, at the very low Q^2, which are of interest to the present work, the replacement of the Feshbach correction is not very relevant, despite the fact that the Feshbach correction ignores magnetic effects.

We perform fits to subsets of the MAMI data of variable length, starting from the lowest available Q^2 value up to some chosen cutoff Q^2_{max} values. Depending on our choice of Q^2_{max}, there are still either four or five normalization constants that must also be determined by the fits. Our fits float these normalization constants, along with the one remaining constant R_p (the only one that cannot be determined from chiral perturbation theory). In all cases, the fits return normalization constants near unity (within 0.5% in all cases, i.e., well within the 2% absolute normalization uncertainty of the measurements).

Figure 1 shows a typical fit used in this work. Shown in that plot are the experimental MAMI measurements [scaled to give σ_{red}, as in Eq. (4)], with the magnetic form factor contribution $(\tau/\epsilon)G_M^2$ (as calculated from chiral perturbation theory—Eq. (6) and Table I) subtracted out. This difference is an estimate of G_E^2, and the derivative of this quantity with respect to Q^2 at $Q^2 = 0$ gives the value of R_p, as indicated in Eq. (3).

The data shown in the figure represent 270 measured cross sections, within five data groups (shown by separate symbols), with each data group having a separate floating normalization constant. The fits use the original 270 MAMI measurements and their uncertainties. For clarity of presentation, the figure shows the average of cross sections taken at identical (or nearly identical) Q^2. The fits are performed with the central value predicted for $\langle r^{2k}\rangle_E$ (for $k \geqslant 2$) and $\langle r^{2k}\rangle_M$ (for $k \geqslant 1$), as shown in the final row of Table I. The fits are then repeated for the full range of values for these moments that fall within the uncertainties given in Table I.

The results of the radius R_p from these fits are shown in Fig. 2(a), as a function of Q^2_{max}, the maximum Q^2 data that is included in the fit. The range of Q^2_{max} used is limited at the lower end by the inability to obtain a precise fit using the small amount of MAMI data with very low Q^2. At the upper end it is limited by three concerns. First, we wish to stop well before $Q^2 = 0.078$ GeV^2, where, due to the charged-pion threshold (at $Q^2 = -0.078$ GeV^2), the Taylor series is no longer meaningful. Second, we restrict ourselves to Q^2_{max} values that give fits with a reduced χ^2 of unity or better. Third, we are restricted by the fact that the uncertainty in the chiral perturbation theory predictions for $\langle r^2\rangle_M$ and higher moments makes a precise determination of R_p infeasible at larger Q^2_{max} values. The sensitivity to $\langle r^2\rangle_M$ becomes particularly acute for large scattering angles, which have a small value of ϵ and therefore a large $(\tau/\epsilon)G_M^2$ contribution for the 180-MeV scattering with Q^2 above our range of Q^2_{max}.

The uncertainties in the determination of R_p are due to a combination of the statistical error from the least-squares fit [the central (blue) region in Fig. 2(a)] and the uncertainties in the moments (the largest from $\langle r^2\rangle_M$, but also from higher electric and magnetic moments). Note that the uncertainty in the determined R_p at the left of Fig. 2(a) ($Q^2_{max} = 0.012$ GeV^2, which includes 118 MAMI cross sections) is dominated by the statistical uncertainty associated with the least-squares fit. The value here is

$$\begin{aligned} R_p &= 0.8538(104)_f(42)_{M2}(35)_{E4}(1)_{M4}(2)_{E6}\ \text{fm} \\ &= 0.8538(117)\ \text{fm}. \end{aligned} \tag{7}$$

Here the f subscript indicates the fit uncertainty, and the $M2$, $E4$, $M4$, and $E6$ subscripts indicate the uncertainties that result from the uncertainties in the moments of Table I (in the second row). The uncertainty at the right side of Fig. 2(a) ($Q^2_{max} = 0.023$ GeV^2, which is a fit of 270 measured MAMI cross sections) is dominated by the Table I uncertainties:

$$\begin{aligned} R_p &= 0.8566(53)_f(78)_{M2}(59)_{E4}(4)_{M4}(6)_{E6}\ \text{fm} \\ &= 0.8566(112)\ \text{fm}. \end{aligned} \tag{8}$$

The fact that the uncertainties at the two ends are dominated by different concerns, and the fact that the values agree at both ends, adds strength to our determination. We average the values at the two ends to obtain our final determination of R_p:

$$R_p = 0.855(11)\ \text{fm}, \tag{9}$$

where the uncertainty is chosen to be consistent with the whole range of Q^2_{max} shown in Fig. 2(a). This range is shown by the dashed lines in Fig. 2(a).

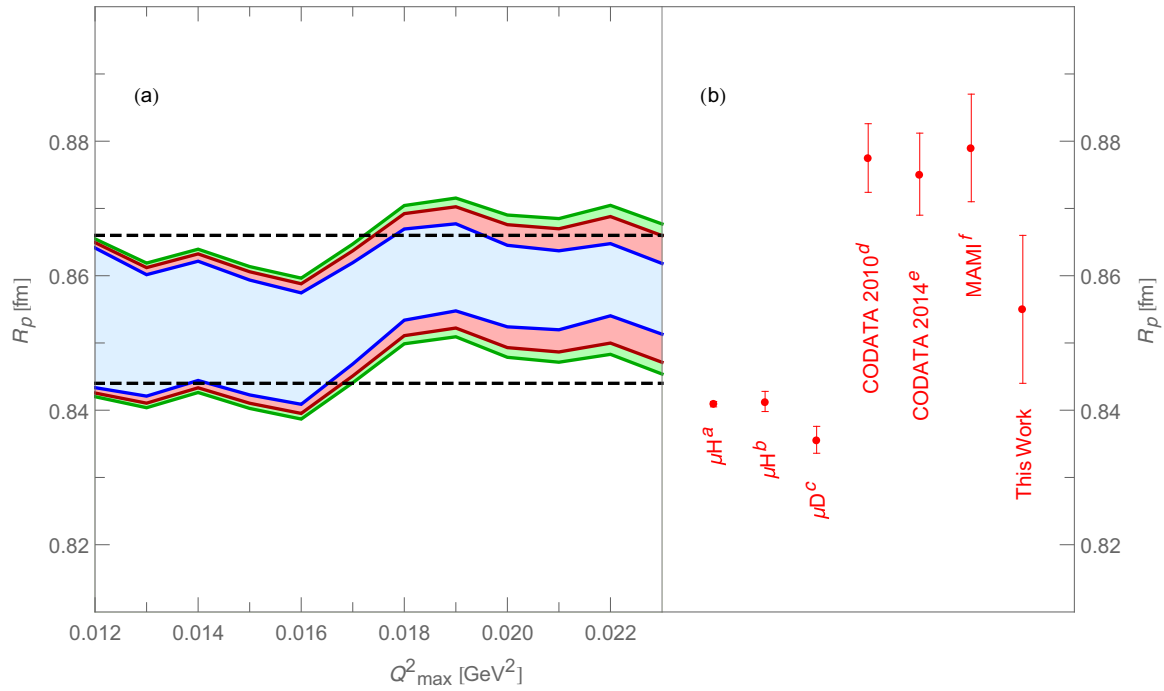

FIG. 2. (a) The range of R_p allowed by the fits as a function of $Q^2_{\rm max}$. The central (blue) region is the range of uncertainty from the fits. The expanded (pink) range includes the uncertainty in $\langle r^2\rangle_M$. The largest (green) band includes the uncertainties in all of the higher-order moments, and represents the full uncertainty in the determination. The dashed lines show the 0.855(11)-fm range of Eq. (9), which represents the final result of this work. (b) A comparison of the result of this work to the original (Refs. [1,2][a]) and chiral perturbation theory motivated (Ref. [21][b]) determinations of R_p from muonic hydrogen [1,2] and from muonic deuterium (Ref. [46][c], along with the hydrogen-deuterium $1S$-$2S$ isotope shift of Ref. [47]), CODATA 2010 (Ref. [3][d]) and 2014 (Ref. [4][e]), and the MAMI analysis of their electron-proton elastic-scattering data (Ref. [23][f]).

The value of $\langle r^2\rangle_M$ plays a major role in our determination, as can be seen from the uncertainties labeled $M2$ in Eqs. (7) and (8). Other methods for determining $\langle r^2\rangle_M$ report [22,48–51] larger values than the chiral perturbation theory predictions shown in Table I. The Particle Data Group reports [52] a value of 0.602(38) fm^2 for $\langle r^2\rangle_M$, which is larger (but within the uncertainty limits) of our value of 0.44(16) fm^2 in Table I. Introducing a larger value of $\langle r^2\rangle_M$ into our fit would decrease the value of R_p, bringing it significantly closer to the value obtained from muonic hydrogen.

Our final result is compared to other determinations of R_p in Fig. 2(b). Our value is higher (by 1.2 standard deviations) than the values obtained from muonic hydrogen. It is also higher (by 1.7 standard deviations) than the value that can be determined from a combination of a muonic deuterium [46] measurement along with a hydrogen-deuterium isotope shift measurement [47]. On the other hand, it is lower than the CODATA value by 1.6 standard deviations and the MAMI prediction by 1.7 standard deviations.

The uncertainty in our determination of R_p [Eq. (9)] is an order of magnitude larger than that of Eq. (2). One side effect of this fact is that we do not have to concern ourselves with a possible different definition for the proton radius (see the discussion in Ref. [11]), because the difference is smaller than the precision we have obtained here.

In summary, we have used chiral perturbation theory inputs, along with fits of the precise MAMI electron-proton elastic-scattering cross sections, to determine the root-mean-square charge radius of the proton: $R_p = 0.855(11)$ fm. This result falls between the determinations of R_p obtained from muonic hydrogen [Eqs. (1) and (2)] and the CODATA value. This work is a step on the path to resolving the proton radius puzzle. The work presented here should be directly applicable to the analysis of ongoing and planned measurements [53] of elastic-scattering cross sections at very low Q^2.

This work was supported in part by Spanish Grants No. FPA2014-55613-P and No. FPA2013-43425-P, by Catalan Grant No. SGR2014-1450, and by the NSERC and CRC of Canada.

APPENDIX

The electric and magnetic Sachs form factors can be written in the following form in the chiral limit ($x^2 = Q^2/m_\pi^2$):

$$G_E(Q^2) = 1 - \frac{R_p^2}{3!}Q^2 + \frac{m_\pi^2}{288\pi^2 F_\pi^2}\left\{3\sqrt{\frac{4}{x^2}+1}\left[4+x^2+g_A^2(8+5x^2)\right]\mathrm{ArcCsch}\left[\frac{2}{x}\right] - 12 - 4x^2 - g_A^2(24+17x^2)\right\}, \quad \text{(A1)}$$

$$G_M(Q^2) = \mu_p - \frac{g_A^2 m_p m_\pi}{32\pi F_\pi^2}\left\{ -2 + \left(\frac{4}{x} + x\right)\mathrm{ArcTan}\left[\frac{x}{2}\right]\right\}. \tag{A2}$$

For $k \geqslant 1$ we have the following expression for the magnetic moments (which, in addition to the pure chiral result, also incorporates the corrections associated with the Δ particle):

$$\begin{aligned}\langle r^{2k}\rangle_M = \frac{(-1)^k(2k+1)!}{2\mu_p}\frac{1}{m_\pi^{2k-1}}\frac{m_p}{\pi F_\pi^2}\Bigg\{ &-\frac{g_A^2(-1)^k}{4^{k+1}(1-4k^2)} + \frac{g_{\pi N\Delta}^2 z^{-1}}{9\pi}\Bigg[\frac{(-1)^{k+1}\Gamma^2(k+1)}{k\Gamma(2k+2)} \\ &+ \frac{2}{4^k(1-4k^2)}\sqrt{1-z^2}\left(\frac{z^2}{1-z^2}\right)^k \ln\left(\frac{2}{z}\right) + (-1)^k\sqrt{1-z^2}\frac{\Gamma^2(k+1)}{\Gamma(2k+2)}\sum_{s=0}^{k-1}\frac{1}{k-s}\left(\tfrac{1}{2}\atop s\right)\left(\frac{z^2}{1-z^2}\right)^s \\ &- (-1)^k\sqrt{1-z^2}\left(\tfrac{1}{2}\atop k\right)\left(\frac{z^2}{1-z^2}\right)^k\frac{\Gamma^2(k+1)}{\Gamma(2k+2)}\sum_{s=1}^{\infty}\frac{(2s)!z^{2s}\,{}_2F_1\left(-k,-s;\frac{3}{2}-k;1-\frac{1}{z^2}\right)}{2^{2s}s(s!)^2}\Bigg]\Bigg\},\end{aligned} \tag{A3}$$

where $z = m_\pi/\Delta$, $\Delta = m_\Delta - m_p$, ${}_2F_1$ is the hypergeometric function, and $\Gamma(n)$ is the Euler Γ function. The numerical values for the masses and the coupling constants are taken from Ref. [43], except for $g_A = 1.2723(23)$, which we take from Ref. [52], and $g_{\pi N\Delta} = 3/(2\sqrt{2})g_A = 1.35$, which we have fixed to the large-N_c prediction.

Note that the z^{-1} terms cancel in the total sum and the general structure of the moments is the following,

$$\langle r^{2k}\rangle_M \sim \frac{1}{m_\pi^{2k-1}}\left[1 + \mathcal{O}\left(\frac{m_\pi}{\Delta}\right)\right], \tag{A4}$$

up to single logarithms, as it should.

[1] R. Pohl *et al.*, Nature **466**, 213 (2010).
[2] A. Antognini, F. Nez, K. Schuhmann, F. D. Amaro, F. Biraben, J. M. R. Cardoso, D. S. Covita, A. Dax *et al.*, Science **339**, 417 (2013).
[3] P. J. Mohr, B. N. Taylor, and D. B. Newell, Rev. Mod. Phys. **84**, 1527 (2012).
[4] P. J. Mohr, D. B. Newell, and B. N. Taylor, Rev. Mod. Phys. **88**, 035009 (2016).
[5] K. Pachucki, Phys. Rev. A **60**, 3593 (1999).
[6] A. P. Martynenko, Phys. At. Nucl. **69**, 1309 (2006).
[7] C. E. Carlson and M. Vanderhaeghen, Phys. Rev. A **84**, 020102 (2011).
[8] M. C. Birse and J. A. McGovern, Eur. Phys. J. A **48**, 120 (2012).
[9] M. Gorchtein, F. J. Llanes-Estrada, and A. P. Szczepaniak, Phys. Rev. A **87**, 052501 (2013).
[10] R. J. Hill and G. Paz, Phys. Rev. Lett. **107**, 160402 (2011).
[11] A. Pineda, Phys. Rev. C **71**, 065205 (2005).
[12] D. Nevado and A. Pineda, Phys. Rev. C **77**, 035202 (2008).
[13] C. Peset and A. Pineda, Eur. Phys. J. A **51**, 32 (2015).
[14] C. Peset and A. Pineda, Nucl. Phys. B **887**, 69 (2014).
[15] J. M. Alarcon, V. Lensky, and V. Pascalutsa, Eur. Phys. J. C **74**, 2852 (2014).
[16] E. E. Jenkins and A. V. Manohar, Phys. Lett. B **255**, 558 (1991).
[17] W. E. Caswell and G. P. Lepage, Phys. Lett. B **167**, 437 (1986).
[18] A. Pineda and J. Soto, Nucl. Phys. Proc. Suppl. **64**, 428 (1998).
[19] A. Pineda and J. Soto, Phys. Lett. B **420**, 391 (1998).
[20] A. Pineda and J. Soto, Phys. Rev. D **59**, 016005 (1998).
[21] C. Peset and A. Pineda, Eur. Phys. J. A **51**, 156 (2015).
[22] J. C. Bernauer, P. Achenbach, C. Ayerbe Gayoso, R. Böhm, D. Bosnar, L. Debenjak, M. O. Distler, L. Doria, A. Esser, H. Fonvieille, J. M. Friedrich, J. Friedrich, M. Gómez Rodrguez de la Paz, M. Makek, H. Merkel, D. G. Middleton, U. Müller, L. Nungesser, J. Pochodzalla, M. Potokar, S. Sánchez Majos, B. S. Schlimme, S. Širca, Th. Walcher, and M. Weinriefer (A1 Collaboration), Phys. Rev. Lett. **105**, 242001 (2010).
[23] J. C. Bernauer, M. O. Distler, J. Friedrich, Th. Walcher, P. Achenbach, C. A. Gayoso, R. Böhm, D. Bosnar, L. Debenjak, L. Doria, A. Esser, H. Fonvieille, M. Gómez Rodríguez de la Paz, J. M. Friedrich, M. Makek, H. Merkel, D. G. Middleton, U. Müller, L. Nungesser, J. Pochodzalla, M. Potokar, S. Sánchez Majos, B. S. Schlimme, S. Širca, and M. Weinriefer (A1 Collaboration), Phys. Rev. C **90**, 015206 (2014).
[24] M. Horbatsch and E. A. Hessels, Phys. Rev. C **93**, 015204 (2016).
[25] K. Griffioen, C. Carlson, and S. Maddox, Phys. Rev. C **93**, 065207 (2016).
[26] D. W. Higinbotham, A. A. Kabir, V. Lin, D. Meekins, B. Norum, and B. Sawatzky, Phys. Rev. C **93**, 055207 (2016).
[27] I. T. Lorenz and U. G. Meißner, Phys. Lett. B **737**, 57 (2014).
[28] I. T. Lorenz, Ulf-G. Meissner, H. W. Hammer, and Y. B. Dong, Phys. Rev. D **91**, 014023 (2015).
[29] G. Lee, J. R. Arrington, and R. J. Hill, Phys. Rev. D **92**, 013013 (2015).
[30] J. C. Bernauer, dissertation, Johannes Gutenberg-Universität, Mainz, 2010.
[31] J. Arrington, Phys. Rev. Lett. **107**, 119101 (2011).
[32] J. C. Bernauer, P. Achenbach, C. Ayerbe Gayoso, R. Böhm, D. Bosnar, L. Debenjak, M. O. Distler, L. Doria, A. Esser, H. Fonvieille, J. M. Friedrich, J. Friedrich, M. Gómez Rodríguez de la Paz, M. Makek, H. Merkel, D. G. Middleton, U. Müller, L. Nungesser, J. Pochodzalla, M. Potokar, S. Sánchez Majos, B. S. Schlimme, S. Širca, Th. Walcher, and M. Weinriefer (A1 Collaboration), Phys. Rev. Lett. **107**, 119102 (2011).

[33] I. T. Lorenz, H.-W. Hammer, and Ulf-G. Meißner, Eur. Phys. J. A **48**, 1 (2012).
[34] I. Sick, Prog. Part. Nucl. Phys. **67**, 473 (2012).
[35] R. Pohl, R. Gilman, G. A. Miller, and K. Pachucki, Annu. Rev. Nucl. Part. Sci. **63**, 175 (2013).
[36] C. Adamuščín, E. Bartoš, S. Dubnička, and A. Z. Dubničková, Nucl. Phys. B, Proc. Suppl. **245**, 69 (2013).
[37] E. Kraus, K. E. Mesick, A. White, R. Gilman, and S. Strauch, Phys. Rev. C **90**, 045206 (2014).
[38] C. E. Carlson, Prog. Part. Nucl. Phys. **82**, 59 (2015).
[39] J. Arrington and I. Sick, J. Phys. Chem. Ref. Data **44**, 031204 (2015).
[40] S. Pacetti, R. B. Ferroli, and E. Tomasi-Gustafsson, Phys. Rep. **550-551**, 1 (2015).
[41] J. Gasser, M. E. Sainio, and A. Svarc, Nucl. Phys. B **307**, 779 (1988).
[42] V. Bernard, N. Kaiser, J. Kambor, and U. G. Meissner, Nucl. Phys. B **388**, 315 (1992).
[43] V. Bernard, H. W. Fearing, T. R. Hemmert, and U. G. Meissner, Nucl. Phys. A **635**, 121 (1998); **642**, 563 (1998).
[44] D. Borisyuk and A. Kobushkin, Phys. Rev. C **86**, 055204 (2012).
[45] D. Borisyuk and A. Kobushkin, Phys. Rev. C **75**, 038202 (2007).
[46] R. Pohl, F. Nez, L. M. P. Fernandes *et al.* (CREMA Collaboration), Science **353**, 669 (2016).
[47] C. G. Parthey, A. Matveev, J. Alnis, R. Pohl, T. Udem, U. D. Jentschura, N. Kolachevsky, and T. W. Hänsch, Phys. Rev. Lett. **104**, 233001 (2010).
[48] B. Kubis and Ulf.-G. Meißner, Nucl. Phys. A **679**, 698 (2001).
[49] T. Bauer, J. C. Bernauer, and S. Scherer, Phys. Rev. C **86**, 065206 (2012).
[50] M. A. Belushkin, H. W. Hammer, and Ulf-G. Meissner, Phys. Rev. C **75**, 035202 (2007).
[51] M. Hoferichter, B. Kubis, J. Ruizde Elvira, H.-W. Hammer, and U.-G. Meißner, Eur. Phys. J. A **52**, 331 (2016).
[52] C. Patrignani *et al.* (Particle Data Group), Chin. Phys. C **40**, 100001 (2016).
[53] C. Peng and H. Gao (PRad collaboration), EPJ Web of Conf. **113**, 03007 (2016).